Evaluating Client Protein Recovery by the Hsp40s DNAJB8 and DNAJB1 with AP-MS

Maureen R. Montoya, Guy M. Quanrud, Liangyong Mei, José L. Montaño, and Joseph C. Genereux[*]

Department of Chemistry, University of California, Riverside, CA 92521

*Joseph C. Genereux, E-mail: josephg@ucr.edu

Keywords: Hsp40; DNAJB1; DNAJB8; AP-MS; misfolded proteins; proteomics

ABSTRACT

Hsp40s play a central role in cellular protein homeostasis by promiscuously surveying the proteome for misfolded proteins. These misfolded client proteins are then delivered to Hsp70. Mutation of the Hsp40 J-domain blocks Hsp70 binding, inhibiting client protein release from Hsp40. We previously integrated misfolded protein recognition by Hsp40 into a platform to identify proteins that are destabilized by cellular stress. However, the dependences of Hsp40 interactions and client recovery on J-domain activity, Hsp40 identity, and crosslinking have not been addressed. Herein, we apply quantitative proteomics to systematically characterize the interactions networks of human Hsp40s DNAJB8 and DNAJB1 with intact or inactivated J-domains. We find that DNAJB8 irreversibly binds over a thousand protein interactors even in the absence of stress. Inactivation of the J-domain decreases interaction with Hsp70 family and associated proteins, but does not generally affect client binding. By contrast, J-domain inactivation and cellular crosslinking substantially increase the relative recovery of proteins from DNAJB1 co-immunoprecipitation. This advantage is completely offset by loss of DNAJB1 recovery under these conditions, making DNAJB1 a poor bait for client protein recovery as compared to DNAJB8. The J-domain inactivated DNAJB8^{H31Q} has increased affinity to its client proteins under heat stress, while no such change in affinity is observed for the wild-type protein, despite their similar client binding profiles under basal conditions. Hence, we find that DNAJB8^{H31Q} is an effective recognition element for the recovery of destabilized client proteins following cellular stress. Raw mass spectrometry data is accessible through the PRIDE archive (pxd030633).

INTRODUCTION

Protein folding to the native state is necessary both to achieve appropriate protein function and to avoid dysfunction due to the accumulation of misfolded and aggregated proteins[1]. To prevent misfolded protein accumulation, chaperones survey the proteome for misfolded and aggregated conformations[2,3]. Holdases, such as the small heat shock proteins (sHSPs), can bind to and segregate misfolded proteins, while ATP-dependent chaperoning can additionally unfold misfolded proteins and assist with proper folding.

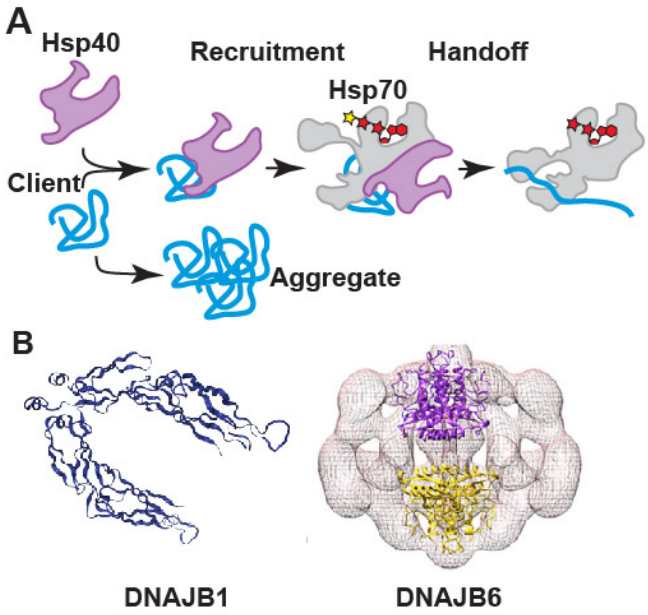

Figure 1. A. Schematic depicting recognition of misfolded client proteins by Hsp40, and their recruitment and handoff to Hsp70. B. Crystal structure of the DNAJB1 dimer[4] and electron microscopy image of DNAJB6 oligomers from Söderberg *et al*, with XL-MS determined dimers fit to EM electron density[5]. DNAJB6 is structurally similar to DNAJB8 and reversibly forms dimers and oligomers in vitro[5–9], with a mixture of monomer, dimers, and oligomers in cells[10].

Among the most ubiquitous and highly conserved chaperoning systems is the Hsp70 chaperone family[11,12]. Hsp70s recognized and assist about a third of the proteome even under basal conditions, and play important roles in diverse cellular pathways including membrane translocation, protein degradation, DNA damage repair, and endocytosis. This functional diversity and promiscuous substrate scope is supported by diverse post-translational modifications and an active co-chaperone network[13,14]. Dozens of different Hsp40s recognize destabilized proteins, recruit them to Hsp70, and stimulate Hsp70 ATP hydrolysis to increase Hsp70-client binding (**Figure 1A**)[15–17]. This process is driven by binding of the

Hsp40 J-domain to Hsp70, which promotes Hsp70 hydrolysis and client transfer to Hsp70. Nucleotide exchange factors promote client release from Hsp70, and scaffolding proteins coordinate client hand-off to other chaperoning systems, such as Hsp90[11,12].

Chaperone affinity for clients can be used as a proxy for destabilization[18,19]. We have exploited the broad substrate scope of Hsp40 to profile protein destabilization in cells exposed to heavy metals[20]. In this assay, the human Hsp40 DNAJB8 is expressed with an N-terminal Flag epitope tag for immunoprecipitation. We introduced the H31Q mutation into the DNAJB8 J-domain to prevent Hsp70 binding. Co-immunoprecipitated proteins are quantified by mass spectrometry using isobaric TMT labeling. We found that proteins that co-immunoprecipitate with ^{Flag}DNAJB8^{H31Q} are generally destabilized compared to the bulk proteome[21]. We used this Hsp40 affinity assay to identify proteins that are destabilized by brief cellular arsenite exposure, finding a series of known arsenite targets, and validated their destabilization by limited proteolysis. However, we chose DNAJB8 based on its lack of expression in our model cell line, HEK293T. We did not know whether all Hsp40 proteins would work well in the assay, nor how J-domain mutation or crosslinking might affect the client recovery by Hsp40 immunoprecipitation. A recent report found that the DNAJB8 J-domain competes with client proteins for the client binding site, suggesting that J-domain inactivation and consequent lack of Hsp70 binding might decrease client interactions through increasing the energetic penalty[10]. Unlike traditional dimeric Hsp40s, such as DNAJB1, DNAJB8 forms large oligomers that could impact client recovery (**Figure 1B**).

Herein we compare client and co-chaperone recoveries between two Class B Hsp40 proteins, DNAJB8 and DNAJB1, along with the effects of intracellular crosslinking and J-domain mutation. We find that DNAJB8 is much more effective than DNAJB1 at isolated clients as opposed to co-chaperones. For both chaperones, J-domain mutation has only a modest effect on client profiles, and although crosslinking increases the stoichiometry of most clients to Hsp40, this increased stoichiometry is more than offset by lowered Hsp40 recovery. Finally, even though DNAJB8^{WT} and DNAJB8^{H31Q} are both effective at isolating clients even in the presence of stringent washing, only DNAJB8^{H31Q} increases client

recovery during heat shock, indicating that it is a preferred tool for profiling stress-dependent protein destabilization.

MATERIALS AND METHODS

Reagents. Biochemical reagents and buffer components were purchased from Fisher Scientific, VWR, or Millipore Sigma. Millipore water and sterilized consumables were used for all biochemical experiments.

Molecular Cloning. DNAJB1 was amplified from cDNA derived from HEK293T cells (ATCC) using TRIzol (Thermo Fisher Scientific) and inserted into the pFlag.CMV2 vector by PIPE cloning[22] using Q5 polymerase and the primers:

5' - CAGATCTATCGATGAATTCGCTATTGGAAGAACCTGCTCAAG -3',

5' - CTTGAGCAGGTTCTTCCAATAGCGAATTCATCGATAGATCTG - 3',

5' - GTAGTAGTCTTTACCCATGACCTTGTCGTCATCGTCTTTG - 3', and

5'- CAAAGACGATGACGACAAGGTCATGGGTAAAGACTACTAC - 3'. The H32Q mutation was introduced into DNAJB1 using site-directed mutagenesis with the oligonucleotides 5'-CTACCAACCGGACAAGAACAAGGAGCCCGG-3' and 5'-CCGGTTGGTAGCGCAGCGCC-3'. ^{Flag}DNAJB8^{WT}.CMV2, and ^{Flag}DNAJB8^{H31Q}.CMV2, and EGFP.pDest30 have been reported[21,23]. Constructs were analytically digested and sequenced (Retrogen) to confirm identity. All cloning enzymes and buffers were purchased from New England Biolabs and primers were purchased from IDT.

Human Tissue Culture. These experiments were performed in HEK293T, which do not represent any specific human tissue type. However, proteostasis mechanisms tend to be highly conserved across euploidal cell lines. Therefore it is likely that the general observations made here will hold, although specific clients might be handled differently. HEK293T cells were cultured in DMEM (Corning) supplemented with 10% fetal bovine serum (FBS; Seradigm), 2 mM L-Glutamine (Corning), and penicillin-streptomycin (100 IU/mL,100 μg/mL; Corning). Cells were transfected with plasmid DNA by the calcium phosphate method. Every experiment involving DNAJB8 used one 10 cm plate per condition.

4-plex experiments involving DNAJB1 used two 10 cm plates per condition to account for its lower expression.

Immunoprecipitation. Cells were harvested from confluent dishes at 36 h to 48 h post-transfection. If crosslinking was used, cells were incubated in the indicated concentration of freshly prepared dithiobis succinimidyl propionate (DSP) in 1% DMSO/PBS for 30 min with rotation at ambient temperature, and then quenched by addition of Tris pH 8.0 (to 90 mM final concentration) and rotation for 15 min. After crosslinking, or directly after harvest for experiments without crosslinking, cells were lysed for 30 min on ice in lysis buffer supplemented with fresh 1 x protease inhibitor cocktail (Roche). Unless otherwise indicated, lysis was performed in RIPA buffer (150 mM NaCl, 50 mM Tris pH 7.5, 1% Triton X100, 0.5% sodium deoxycholate, 0.1 % SDS). For low stringency experiments using DNAJB1, lysis was performed with 0.1% Triton x-100 in TBS (10 mM Tris pH 7.5, 150 mM NaCl). Lysate was separated from cell debris by centrifugation at 21,100 x g for 15 min at 4 °C. Protein was quantified by Bradford assay (Bio-Rad). Lysates were pre-cleared with 15 µL sepharose-4B beads (Millipore Sigma) for 30 min at 4 °C, followed by immunoprecipitation with 15 µL M2 anti-FLAG Magnetic Beads (Millipore Sigma) and overnight rotation at 4°C. Beads were washed four times with lysis buffer the next day for DNAJB8 or three days later for DNAJB1. Proteins were eluted from the beads by boiling in 30 µL of Laemmli concentrate (120 mM Tris pH 6.8, 60% glycerol, 12% SDS, brilliant phenol blue to color). About 17% of each eluate was reserved for silver stain analysis, and the remainder prepared for mass spectrometry.

Silver Stain. Eluates were boiled for 5 min at 100 °C with 0.17 M DTT, loaded into 1.0 mm, 12% polyacrylamide gels, and separated by SDS-PAGE. Gels were rinsed in Millipore water for 5 min. Gels were left overnight in fixing solution (10% acetic acid, 30% ethanol), washed 3 x 20 min in 35% ethanol, sensitized (0.02% sodium thiosulfate) for 2 min, washed with Millipore water 3 x 2 min, and stained for 30 min to overnight in Ag staining solution (0.2% $AgNO_3$, 0.076% formalin). Gels were washed 2 x 1 min with Millipore water and developed (6% sodium carbonate, 0.05% formalin, 0.0004% sodium thiosulfate) until bands reached desired intensity and imaged on a white-light transilluminator (UVP).

TMT-MuDPIT. Immunoprecipitates were prepared for TMT-AP-MS according to standard protocols[24–26]. After TMT labeling, each TMT reaction was quenched with 0.4% ammonium bicarbonate. Labeled digests were combined and fractionated by SCX in line with a reversed-phase analytical column to enable two-dimensional separation prior to electrospray ionization. Peptides were analyzed using a LTQ Orbitrap Velos Pro in data-dependent mode. The top ten peaks from each full precursor scan were fragmented by HCD (stepped collision energies of 36%, 42%, 48% with 100 ms activation time) to acquire fragmentation spectra with 7500 resolving power at 400 m/z. Dynamic exclusion parameters were 1 repeat count, 30 ms repeat duration, 500 exclusion list size, 120 s exclusion duration, and 2.00 Da exclusion width. Files were converted to mzml using ProteoWizard MSConvert[27]. Peptide-spectra matches were evaluated by FragPipe[28,29] against the Uniprot human proteome database (Jun 11, 2021 release, longest entry for each protein) with 20429 sequences (including common contaminants) plus a full reversed sequence decoy set. Cysteine alkylation (+57.02146 Da) and TMT modification (+229.1629 on lysine and N-termini) were set as fixed modifications. Half tryptic and fully tryptic peptides were allowed, as were 2 missed cleavages per peptide. A mass tolerance of 1 Da for precursors and 20 ppm for fragments was allowed. Decoy proteins, non-human contaminants, immunoglobulins, and keratins were filtered from the final protein list.

Gene Ontology. Selective interactors were analyzed by Panther 17.0 (20220202 Release) by comparison to all Homo sapiens genes in the PANTHER GO-Slim Biological Process annotation data set[30]. Ontologies were evaluated by False Discovery Rate based on Fisher's Exact Test.

Statistical Methods. TMT intensity ratios were analyzed using Excel. Box and whisker plots are presented with lines marking median values, X marking average values, boxes from the first to third quartiles, whiskers extending to minimum and maximum values (excluding outliers), and outliers defined at points greater than 1.5-fold the interquartile range beyond the first and third quartiles. Violin plots were generated in R using the ggplot2 library. For bait vs. mock experiments, Pearson's R-derived t-statistics were used for determination of p-values[21]. q-values (q_{BH}) were determined from p-values using Storey's modification of Benjamini-Hochberg's methodology[31,32], and adjusted to maintain monotonicity. For heat

shock experiments with DNAJB8^{H31Q} and DNAJB8^{WT}, integrated TMT reporter ion intensities of identified proteins were normalized to bait intensities.

RESULTS

^{Flag}DNAJB8^{WT} specifically enriches hundreds of proteins in TMT-AP-MS.

To determine the interactor profile of DNAJB8^{WT}, we overexpressed ^{Flag}DNAJB8^{WT} or mock (eGFP) in HEK293T cells, lysed, and immunoprecipitated using the M2 anti-Flag antibody crosslinked to magnetic beads (**Figure 2A** and **Figure S1**). To minimize non-specific interactions, beads were washed well with RIPA buffer, a high detergent solution (150 mM NaCl, 50 mM Tris pH 7.5, 1% Triton X100, 0.5% sodium deoxycholate, 0.1% SDS) developed to break up most protein-protein interactions. Tryptic digests of the eluate were isobarically labeled with TMT tags, quantified by MuDPIT LC-MS, and relative protein abundances inferred from TMT reporter ion ratios for identified peptides. Interaction significance was determined using our previously reported bait correlation method[21].

We identified 2743 proteins from the three runs. Of these proteins, 2623 show preferential recovery in the presence of DNAJB8 with a Storey-Benjamini-Hochberg q-value below 1% (**Figure 2B** and **Table S1**). These proteins are highly enriched in RNA binding proteins (705/1689, GO:0003723). Proteins that are selective for the *absence* of DNAJB8 include KIF11, WDR77, and PRMT5, which are well-characterized binders to anti-Flag antibodies and are prominent in control Flag immunoprecipitations in the CRAPome database[33,34]. Piette *et al* recently reported a careful identification of all human Hsp40 interactors in the cell based on AP-MS experiments and global comparison to controls[35]. They report 34 high-confidence DNAJB8 interactors. We identify 30 of these interactors. DNAJB8 immunoprecipitates several cytosolic Hsp70-associated proteins, including constitutive cytosolic Hsp70 HSPA8, the inducible cytosolic Hsp70s HSPA1A and HSPA6, and cytosolic Hsp70 co-chaperones STUB1, HSPA4, DNAJB1, DNAJB6, and DNAJA2. These strong associations are consistent with the canonical role of Hsp40 proteins as co-chaperones of Hsp70. In addition, the ER Hsp70 HSPA5 and mitochondrial Hsp70 HSPA9 are also recovered (alongside 183 and 112 other mitochondrial and ER proteins respectively), indicating

that DNAJB8 maintains binding to proteins that it encounters after cellular lysis. The large number of associated proteins suggests that DNAJB8^{WT} is at least as competent for recovery of associated clients as DNAJB8^{H31Q}.

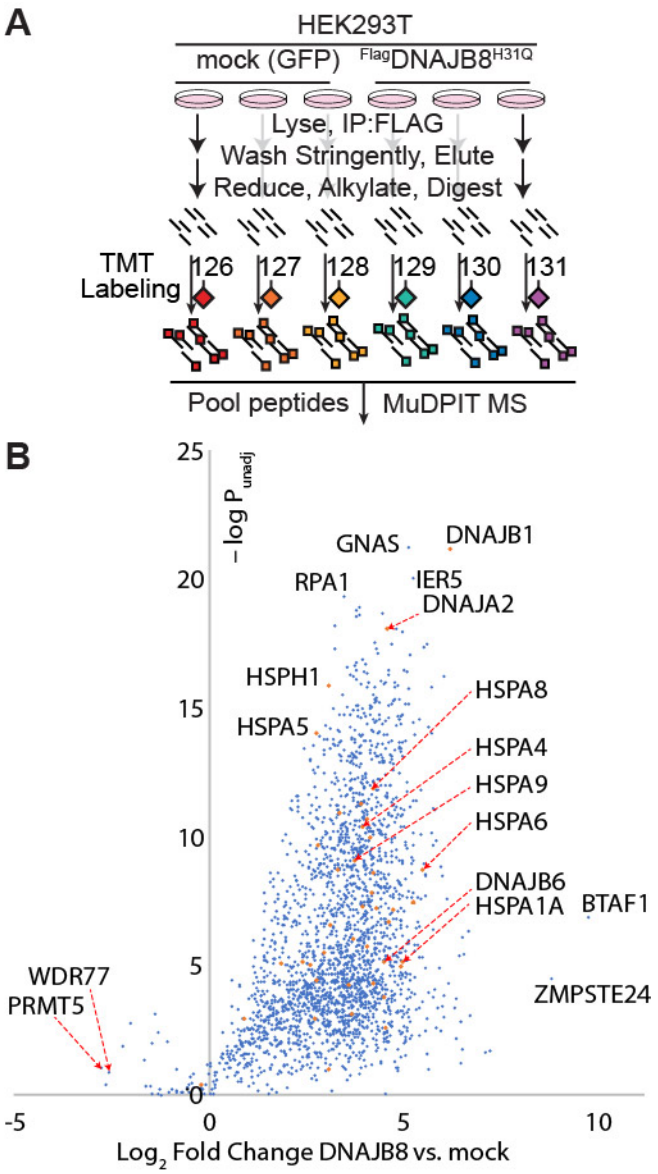

Figure 2: Clients of ^{Flag}DNAJB8^{WT} identified by anti-Flag co-immunoprecipitation from HEK293T cells and TMT-LC-MS. Mock cells are transfected with eGFP. Hsp70 and Hsp70-associated proteins are in orange. Nine biological replicates, comprising three LC-MS runs, were performed. The global false discovery rate for all proteins from Storey's modification of Benjamini-Hochberg analysis is 2.6%.

Influence of crosslinking and J-domain inactivation on DNAJB8 client binding.

Our previous client protein analysis for DNAJB8^{H31Q}, in the presence of crosslinker, found 463 interacting proteins (using $p < 0.05$, fold change > 1.2 vs. mock; 476 with $q < 0.01$). Of these, 251 are shared with DNAJB8^{WT} using the same criteria, while 2183 protein groups were high-confidence interactors with DNAJB8^{WT} without crosslinking but not DNAJB8^{H31Q} with crosslinking. To better understand the role of crosslinking and J-domain inactivation in DNAJB8 interactor recovery, we performed a series of TMT-AP-MS experiments directly comparing the four possible conditions: WT vs. H31Q, and ± crosslinker (**Figure 3A** and **Figure S2A**). For these experiments, we used the reversible crosslinker DSP. DSP is cell-penetrable and allows us to immortalize cellular interactions prior to lysis. After immunoprecipitation and elution, we reverse the crosslinks with TCEP to allow peptide identification during mass spectrometry. Because crosslink yield tends to be low on a per peptide basis, we do not include DSP modification as a variable modification for peptide-spectral matching. An initial optimization did not find meaningful variation in median protein recovery with varying crosslinker concentrations, so we used 1 mM DSP as a standard condition (**Figure S2B,C**). We expected that J-domain mutation would decrease interactions with Hsp70s, and indirectly interactions with Hsp70 co-chaperones, while crosslinking would increase the recovery of most clients by preventing their dissociation during lysis and washing of the beads with RIPA.

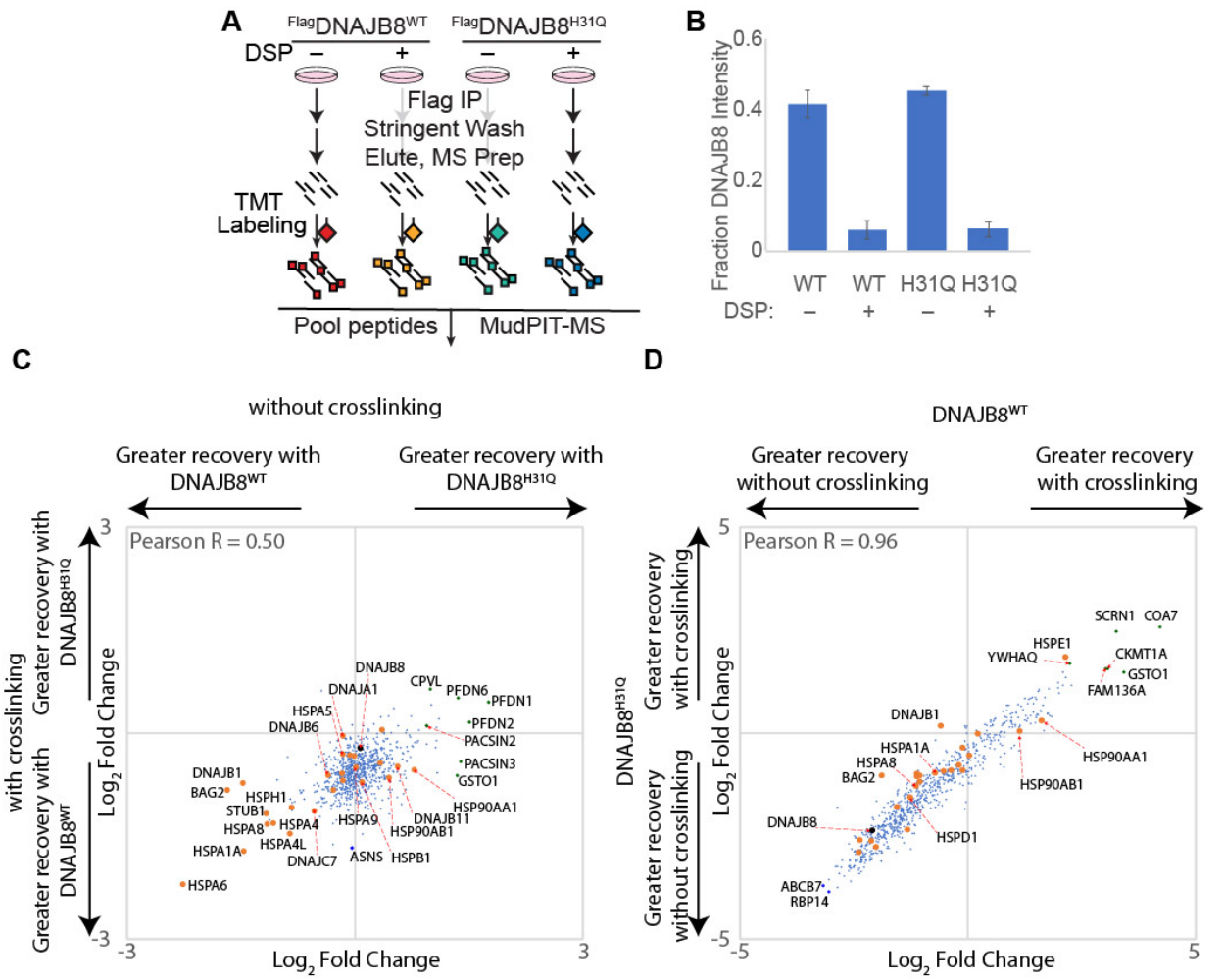

Figure 3: Effect of J-domain integrity and cellular crosslinking on interactor recovery with DNAJB8. A) Schematic of immunoprecipitation. B) Recovery of DNAJB8 from each condition. Error bars represent standard deviation (n = 3). C, D) Relative association of interactors. Hsp70 chaperones and Hsp70-associated co-chaperones are shown in orange. Three biological replicates, comprising three LC-MS runs, were performed.

DNAJB8^{WT} and DNAJB8^{H31Q} have similar expression and immunoprecipitation efficiencies (**Figure 3B** and **Figure S2D,E**). For the most part, J-domain mutation has a modest effect on the interactor profile of DNAJB8 (**Figure 3C**, **Figure S3,** and **Table S2**). As expected, cytosolic Hsp70 chaperones and associated co-chaperones have markedly less affinity for DNAJB8^{H31Q}. This is true both in the presence and absence of crosslinking. By contrast, the ER and mitochondrial Hsp70s (HSPA5, HSPA9), have similar affinity for both DNAJB8s (Figure S3B). The proteins with the strongest preference for DNAJB8^{H31Q} compared to DNAJB8^{WT} are the prefoldins (PFDN1, PFDN2, PFDN6)

(Figure S3B). No such preference is found for components of the prominent prefoldin-associated complexes TRiC and RNA polymerase II, suggesting that the recognized prefoldin complex may not be active.

As expected, crosslinking sharply decreases DNAJB8 levels in the lysate as well as the recovered fraction, by > 80% (**Figure 3B**). Interestingly, crosslinking increases immunoprecipitation efficiency, perhaps by rendering any large DNAJB8-containing complexes insoluble (**Figure S2D,E**). The effect of crosslinking on interactor recovery is almost identical between the DNAJB8 baits, with a Pearson correlation of 0.96 between the two profiles (**Figure 3D, Figure S3,** and **Table S1**). Crosslinking sharply decreases recovery of DNAJB8, and although it increases the recovery of interactors *relative to* DNAJB8, it is not enough to offset the decrease in DNAJB8 bait for most interactors. Exceptions include HSPE1 and a few 14-3-3 proteins, especially 14-3-3θ/YWHAQ (**Figure S3B**). Few proteins show greater relative recovery than DNAJB8 in the absence of crosslinker. In summary, the primary consequence of DNAJB8 J-domain inactivation is to decrease association to Hsp70 family chaperones and co-chaperones, and crosslinking is largely dispensable.

Interactor Recovery by DNAJB1 Immunoprecipitation

Class B Hsp40s are distinguished by an N-terminal J-domain, a glycine/phenylalanine rich domain, two beta-barrel domains, and a C-terminal dimerization domain. For cytosolic Class B Hsp40s, the first beta-barrel includes a weak Hsp70 binding site which is important for client transfer[36]. This class can be further divided into the two phylogenetic trees. In one branch, DNAJB6 and DNAJB8 feature a unique serine/threonine rich region N-terminal to the dimerization domain. This region is implicated in their remarkable ATP-independent holdase activity that substoichiometrically inhibits aggregation of amyloidogenic proteins[7,37,38]. The most abundant Hsp40 of the other branch is DNAJB1, which is also the most well-studied member of the class. DNAJB1 participates in diverse Hsp70-dependent processes, including most notably protein disaggregation, and has limited holdase activity.

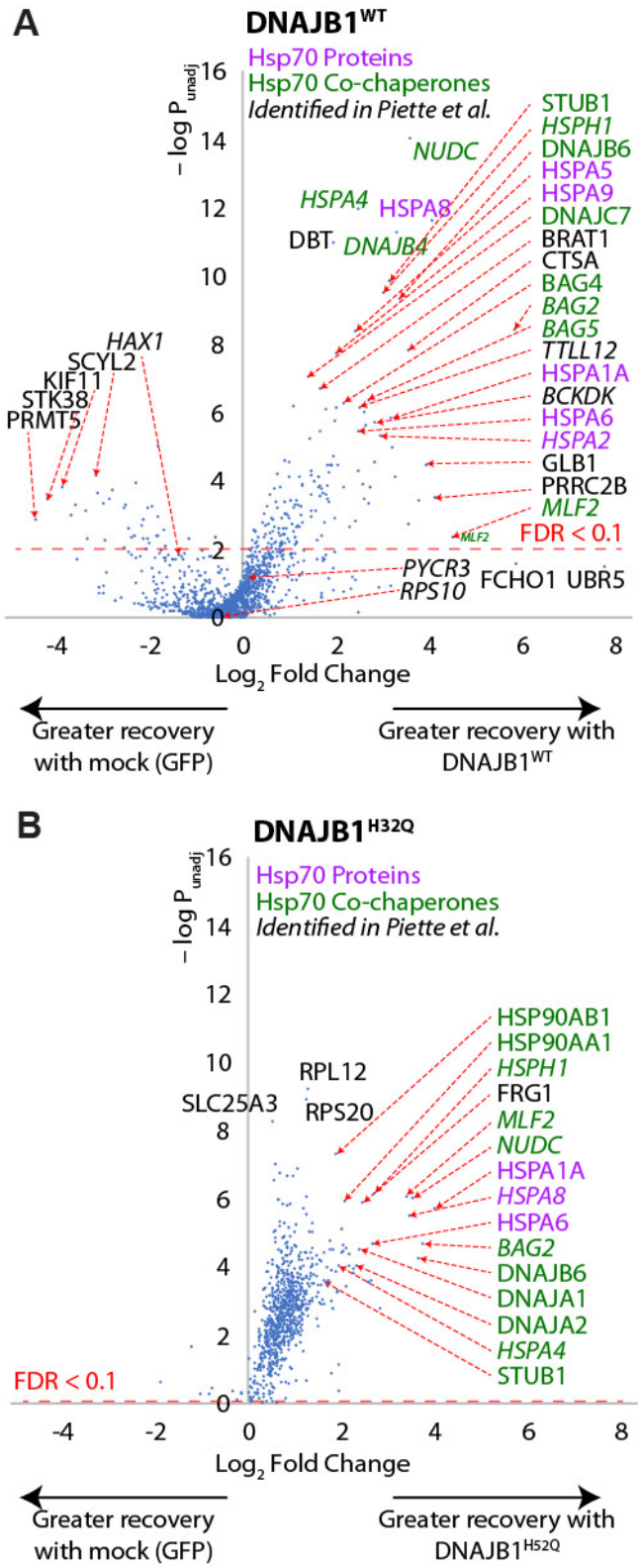

Figure 4. Interactors of ^{Flag}DNAJB1^{WT} (**A**) and ^{Flag}DNAJB1^{H32Q} (**B**) identified by anti-Flag co-immunoprecipitation from HEK293T cells and subsequent TMT-LC-MS. Mock cells are transfected with eGFP. The experimental strategy is similar to that from **Figure 2A**, except that the DNAJB1^{H32Q} AP-MS

was preceded by cellular crosslinking with 250 µM DSP. Nine biological replicates, comprising three LC-MS runs, were performed for DNAJB1^{WT}, while six biological replicates, comprising two LC-MS runs, were performed DNAJB1^{H32Q}. Hsp70 proteins are indicated in purple, Hsp70-associated co-chaperones are in green, and protein identified from Piette *et al*[35] are italicized. The p-value cut-off corresponding to a 10% False Discovery Rate is indicated. The global false discovery rate for all proteins from Storey's modification of Benjamini-Hochberg analysis is 2.6% for DNAJB1^{WT} and 5.9% for DNAJB1^{H32Q}.

We characterized the interaction networks of ^{Flag}DNAJB1^{WT} (in the absence of crosslinking), and ^{Flag}DNAJB1^{H32Q} (in the presence of crosslinking), to determine the interactor profiles (**Figure 4A,B, Figure S4A,** and **Table S3**). The crosslinking concentration was optimized by TMT-AP-MS at varying concentrations of DNAJB1 (**Figure S4B,C**). Although median reporter ion intensities only change modestly with varying [DSP], there was a slight maximum at 0.25 mM DSP. We also found that extending the immunoprecipitation to 3 days increased DNAJB1 recovery (**Figure S4D,E**). DNAJB1 co-immunoprecipitates a much smaller range of proteins as compared to DNAJB8, and the strongest interactors are almost entirely Hsp70s or their associated co-chaperones (**Figure 4A**). 14/14 of the human interactors from Piette *et al*[35] were found, though two (PYCR3, RPS10) did not show meaningful selectivity in our experiment between the presence or absence of DNAJB1^{WT}. 15/33 of Bioplex interactors[39,40] (from HEK293) were identified, of which 4 (PYCR3, HDLBP, MAP2K2, and DIS3) did not show meaningful selectivity. These proteins participate in extensive interaction networks in the Bioplex, and they might lose affinity to DNAJB1 when these networks are disrupted by highly stringent RIPA buffer. As with DNAJB8, common anti-Flag-binding contaminants are depleted in the ^{Flag}DNAJB1 immunoprecipitates. Similar results were observed for DNAJB1^{H32Q}; relatively few proteins were identified compared to DNAJB8, with the strongest interactions dominated by Hsp70 and Hsp70-associated chaperones. Although they could be associating as clients, or as chaperones for any misfolded DNAJB1, the most likely explanation is that DNAJB1^{H32Q} is forming heterodimers with endogenous DNAJB1^{WT}, as well as other DNAJ proteins that still contain a functional J-domain. Such heterodimers have been observed for most Class I and Class II DNAJ proteins[11,41]. Still, DNAJB1^{H32Q} does find some interactors that DNAJB8^{WT} and DNAJB8^{H31Q} miss, and could potentially be useful for extending the client space (**Figure S5**).

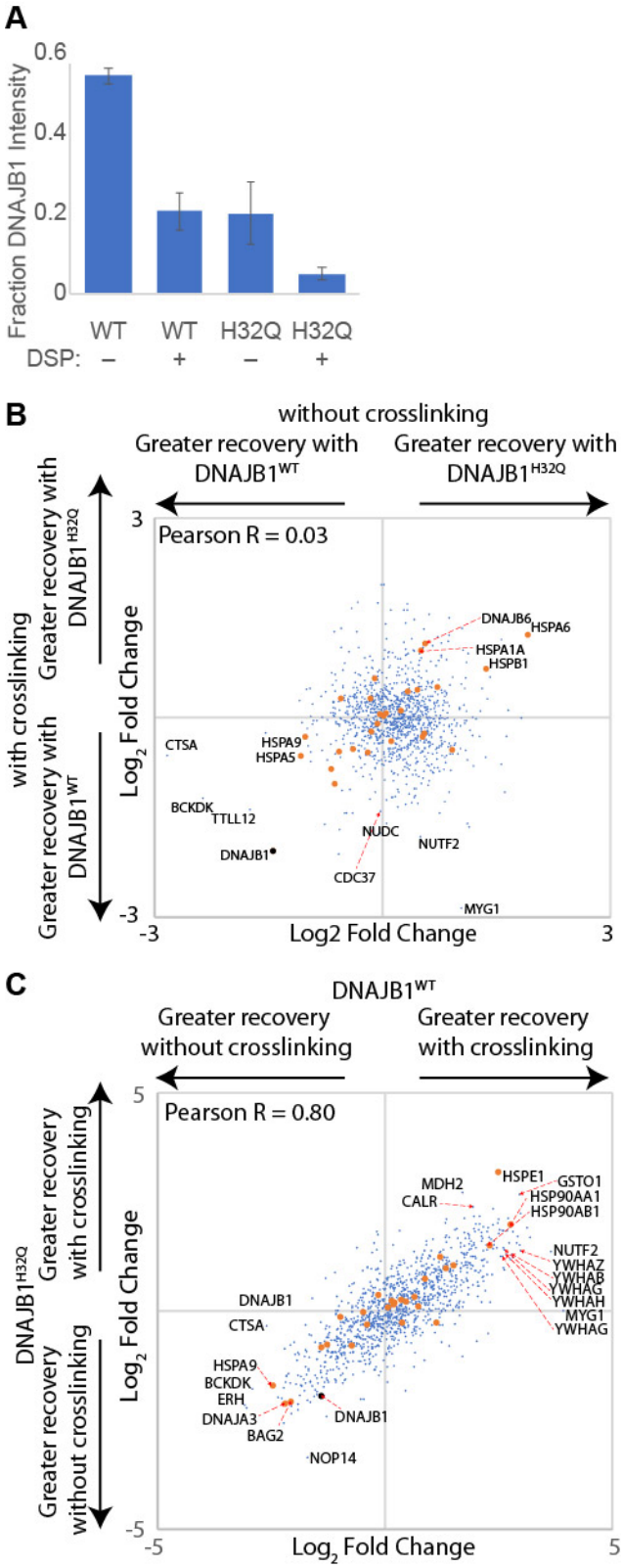
A
Fraction DNAJB1 Intensity
0.6
0.4
0.2
0
WT
WT
H32Q
H32Q
DSP:
–
+
–
+
B
without crosslinking
Greater recovery with DNAJB1WT
Greater recovery with DNAJB1H32Q
with crosslinking
Greater recovery with DNAJB1H32Q
Greater recovery with DNAJB1WT
Pearson R = 0.03
Log2 Fold Change
Log2 Fold Change
3
-3
-3
3
DNAJB6
HSPA6
HSPA1A
HSPB1
CTSA
HSPA9
HSPA5
BCKDK
TTLL12
DNAJB1
NUDC
NUTF2
CDC37
MYG1
C
DNAJB1WT
Greater recovery without crosslinking
Greater recovery with crosslinking
DNAJB1H32Q
Greater recovery with crosslinking
Greater recovery without crosslinking
Pearson R = 0.80
Log2 Fold Change
Log2 Fold Change
5
-5
-5
5
MDH2
CALR
HSPE1
GSTO1
HSP90AA1
HSP90AB1
NUTF2
YWHAZ
YWHAB
YWHAG
YWHAH
MYG1
YWHAG
DNAJB1
CTSA
HSPA9
BCKDK
ERH
DNAJA3
BAG2
DNAJB1
NOP14

Figure 5: Effect of J-domain integrity and cellular crosslinking on interactor recovery with DNAJB1. A) Schematic of immunoprecipitation. B) Recovery of DNAJB1 from each condition. Error bars represent standard deviation (n = 3). C, D) Relative association of interactors. Hsp70 chaperones and Hsp70-associated co-chaperones are shown in orange. Three biological replicates, comprising three LC-MS runs, were performed.

To better understand the role that the J-domain has in DNAJB1 interactor recovery, we directly compared interactor recovery for DNAJB1^{WT} vs. DNAJB1^{H32Q} in both the absence and presence of crosslinking; this is similar to the experiment described in **Figure 3A** for DNAJB8. In contrast to DNAJB8, there is far lower DNAJB1 expression and hence recovery of DNAJB1^{H32Q} as opposed to DNAJB1^{WT} (**Figure 5A**, **Figure S6A,** and **Table S4**). Similar loss of DNAJB1 is observed with crosslinking. For both crosslinking and J-domain inactivation, however, the loss of bait is offset by a corresponding increase in protein recovery relative to DNAJB1 levels, such that overall interactor recoveries are similar across all four conditions (**Figure 5B,C** and **Figure S6B**). Surprisingly, DNAJB1^{H32Q} particularly enriches the inducible cytosolic Hsp70s HSPA6 and HSPA1A, despite lacking a J-domain (**Figure 5B** and **Figure S6B**). The WT protein, on the other hand, preferentially interacts with BCKDK and TTLL12 (**Figure 5B and Figure S6B**). Crosslinking is necessary for recovery of 14-3-3 proteins and Hsp90s, but lowers recovery of BCKDK (**Figure 5C and Figure S6B**). The low overall protein recovery made us consider that perhaps RIPA washing was responsible for removing important interactors. Hence, we performed an identical set of experiments using a gentle lysis and wash buffer (0.1% Triton X100 in TBS). Nearly identical results were obtained, except that overall protein identifications dropped to only 284 proteins (**Figure S7**). This decrease in protein recovery could be due to the low detergent buffer leading to less efficient lysis. While recovery in the DNAJB1^{WT} is unaffected, gentle washing increases protein recovery with DNAJB1^{H32Q} in the absence of crosslinking as opposed to in the presence of crosslinking. Overall, J-domain inactivation and crosslinking are, both individually and combined, effective approaches to increase interactor stoichiometry on DNAJB1. *However*, the low recovery of DNAJB1 itself offsets the greater interactor stoichiometry. This challenge would have to be overcome to make DNAJB1 a useful tool for separation of misfolded cellular proteins.

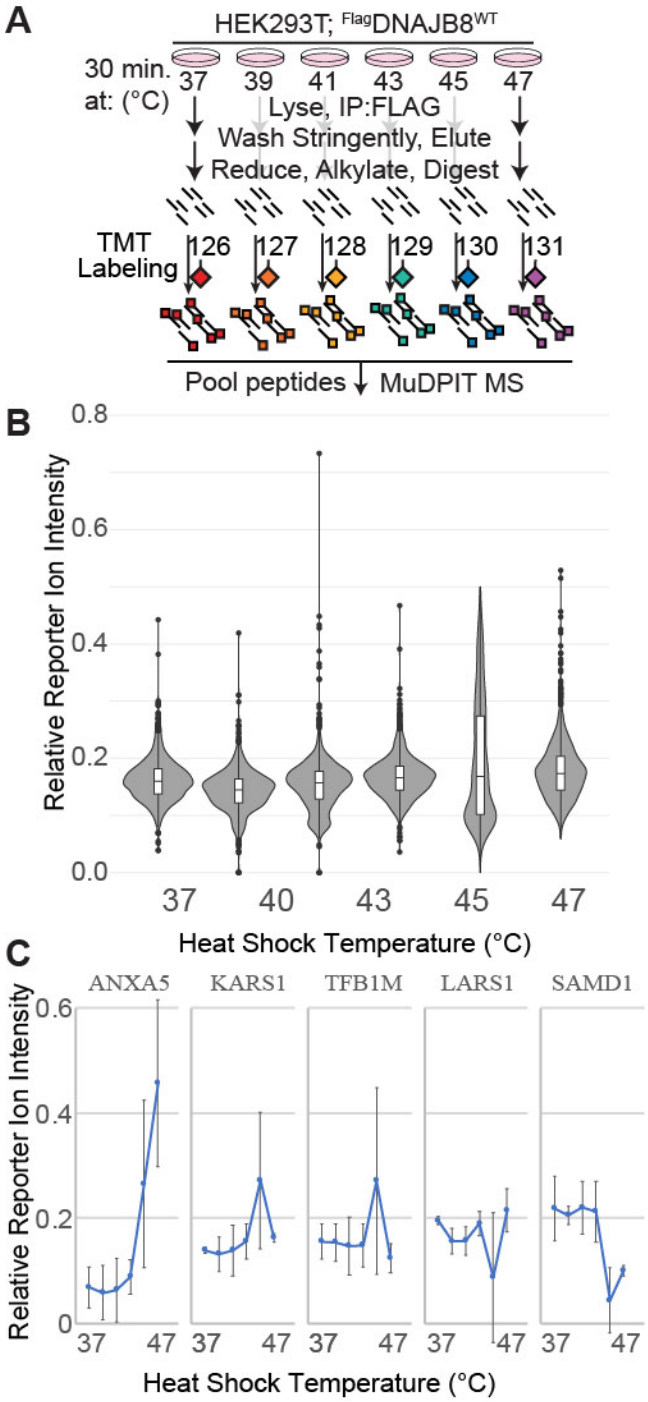

Figure 6. A) Schematic describing the experiment profiling DNAJB8^{WT} affinity following heat shock. B) Violin and bar plots for all quantified interacting proteins (n = 1541). C) Changes in reporter ion intensity for proteins with the highest, 25%, median, 75%, and lowest response with respect to temperature. Error bars represent standard deviation (n = 3).

DNAJB8, on the other hand, demonstrated excellent client recovery, both with and without J-domain inactivation. Furthermore, the binding is strong even without crosslinking and following stringent

washing. Hence, we considered the ability of DNAJB8^{WT} to identify changes in protein stability following a stress. We subjected ^{Flag}DNAJB8^{WT}-expressing HEK293T cells to mild heat stress for 30 min., followed by immediate lysis and anti-Flag immunoprecipitation (**Figure 6A**). The short treatment was chosen to minimize transcriptional/translational remodeling of the cell due to induction of the Heat Shock Response[42,43]. The relative recovery of proteins was determined by MuDPIT LC-MS with isobaric TMT labeling, and integrated reporter ion ratios normalized to the amount of DNAJB8 bait. Surprisingly, we see only modest changes in DNAJB8^{WT} affinity with increasing temperature (**Figure 6B, Figure S8A,B, and Table S5**). Although a few proteins show increased association, most show no change.

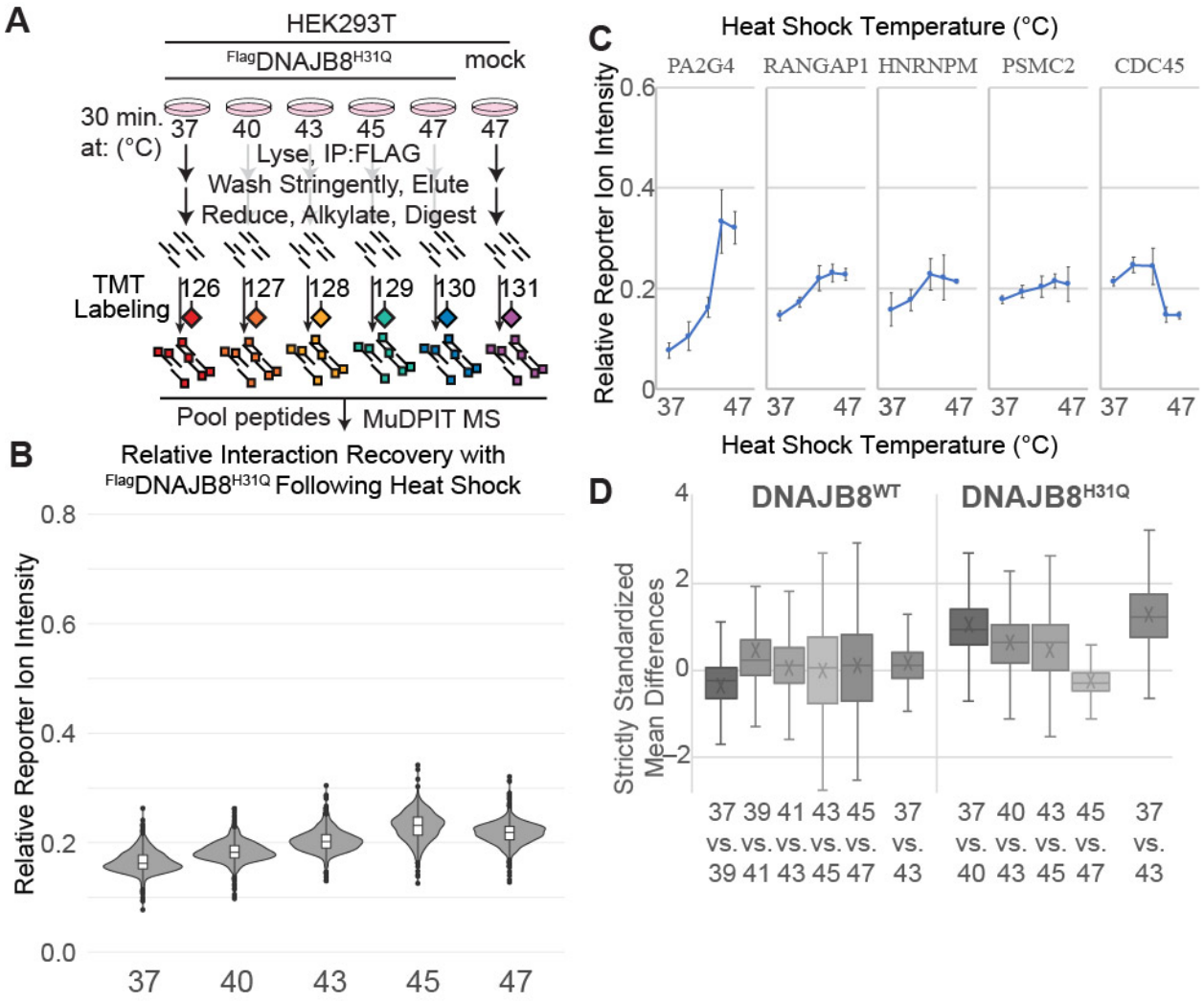

Figure 7. A) Schematic describing the experiment profiling DNAJB8^{H31Q} affinity following heat shock. B) Violin and bar plots for all quantified interacting proteins (n = 989). C) Changes in reporter ion intensity for proteins with the highest, 25%, median, 75%, and lowest response with respect to

temperature. Error bars represent standard deviation (n = 3). D. Box and Whisker plot for Strictly Standardized Mean Differences between consecutive temperatures for DNAJB8 affinity during heat shock. Temperatures below are in units of °C. Outliers outside of the central 50% are not included. 37 °C vs 43 °C is also included as those temperatures were in both sample sets, and starkly demonstrates that DNAJB8^{H31Q} has meaningfully increased affinity for its entire client proteome following heat shock while DNJAB8^{WT} does not.

We performed a similar temperature dependence with ^{Flag}DNAJB8^{H31Q}, this time changing our temperatures to 37 °C, 40 °C, 43 °C, 45 °C, 47 °C to accommodate inclusion of cells expressing mock (eGFP) and heated to 47 °C as a control for misfolding-induced affinity for beads (**Figure 7** and **Figure S8C,D**). Proteins that showed less than 2-fold selectivity for the presence of DNAJB8 were excluded from further analysis (34 protein groups, dominated by the usual anti-Flag binding proteins), leaving 989 protein groups identified and quantified from all three runs. The relationship between temperature and DNAJB8^{H31Q} affinity is a sharp contrast to that observed for DNAJB8^{WT}. For about 80% of the proteome the Hsp40 affinity monotonically increases as the temperature increases from 37 °C to 45 °C, with plateauing or a slight drop-off at 47 °C. For proteins that do not exhibit this trend, there is a tendency to for Hsp40 affinity to increase from 37 °C to 43 °C, followed by a decrease in protein recovery. Although we did not collect sufficient data to estimate transition temperatures, we can estimate the sensitivity of Hsp40 affinity to temperature by taking the response (slope). We compared these slopes to published aggregation temperatures in HEK293T cells as determined by CETSA[44] and melting temperatures in HeLa cells determined from limited proteolysis[45] (**Figure S8E**). No correlation is found (643 protein groups found in both data sets, R = 0.0008).

DISCUSSION

We previously demonstrated that DNAJB8^{H31Q} is effective for profiling the misfoldome in response to cellular stress[20], due to seemingly irreversible binding to its client proteins in the cell. DNAJB1 is one of the best studied Hsp40s due to its high concentration, promiscuous activity, selectivity for misfolded protein, and high similarity to yeast Sis1[15,36,46,47], leading us to consider whether DNAJB1 could be similarly used to recover its cellular clients. We find that DNAJB1^{WT} preferentially associates

with Hsp70 family members, pulling down a far less diverse proteome than DNAJB8 (**Figure S5**), consistent with its primarily ATP (and presumably Hsp70)-dependent biological function. While J-domain inactivation and crosslinking both help increase the relative client load on DNAJB1, they decrease bait recovery so much that any benefit is offset. Hence, DNAJB8 outperforms DNAJB1 in allowing recovery of its clients. However, DNAJB1 does access a distinct proteome from DNAJB8. Hence, DNAJB1 might have potential to supplement client profile by DNAJB8. Furthermore, other class II Hsp40 chaperones with substantial ATP-independent activity such as DNAJB6 or DNAJB2a might also serve as factors to expand the client profile accessible through DNAJB8^{H31Q}.

Given that both DNAJB8^{WT} and DNAJB8^{H31Q} bind strongly to their client proteomes, we expected that heat shock would have a similar effect on protein affinity for both chaperones. This was not the case, as heat shock increases client protein binding to DNAJB8^{H31Q} and not DNAJB8^{WT} (**Figures 6 and 7**). The small change in client affinity for DNAJB8^{WT}, as opposed to DNAJB8^{H31Q}, could be due to the enhanced proteostasis activity following stress. It was recently reported that DNAJB8 interacts with Hsp70 to promote proteasomal degradation of destabilized, aggregation-prone clients[48]. If increased protein association with DNAJB8^{WT} during heat shock also increases the flux of hand-off to Hsp70, then the steady state association of client proteins will only modestly change. DNAJB8^{H31Q}, however, will have impaired hand-off to Hsp70, causing its steady state client load to increase.

The lack of relationship between temperature-dependent affinity for Hsp40 and either melting temperatures determined by CETSA or by limited proteolysis points to the fundamental differences between the techniques. CETSA will only identify loss of proteins that sample conformations that are committed to an aggregation cascade, while limited proteolysis determines local changes in proteolytic susceptibility. A change in conformation that increases solvent exposure, but does not present hydrophobic regions, will register as misfolded by limited proteolysis but not by Hsp40 affinity profiling. However, a conformational change that presents hydrophobic surfaces without affecting the fraction of protein that irreversibly aggregates will lead to a protein hit by Hsp40 affinity profiling but not CETSA. In keeping with these fundamental biophysical differences between the methods, there is also no

correlation between melting temperatures from the published CETSA and limited proteolysis experiments (**Figure S8E**). It should be noted that melting temperatures from CETSA are consistent between experiments; the same HEK293T proteins correlate with CETSA melting temperatures from Jurkat cells determined in 2014 by the same group ($R^2 = 0.42$)[49].

In summary, DNAJB1 and DNAJB8 have been evaluated for their ability to recover cellular clients. We find that DNAJB8^{H31Q} without crosslinking is the most effective approach, and demonstrate that mild heat shock leads to generally monotonic increased affinity of clients with DNAJB8^{H31Q}.

Supporting Information Available. The Supporting Information is available free of charge:

- Supporting Figures S1 through S8, providing silver stains, Western blots, and further analysis of proteomic data (PDF)
- Table S1 providing integrated TMT reporter ions and analysis for DNAJB8^{WT} AP-MS interactors.
- Table S2 providing integrated TMT reporter ions and analysis for AP-MS comparing DNAJB8^{WT} and DNAJB8^{H31Q} with or without crosslinking.
- Table S3 providing integrated TMT reporter ions and analysis for DNAJB1^{WT} and DNAJB1^{H32Q} AP-MS interactors.
- Table S4 providing integrated TMT reporter ions and analysis for AP-MS comparing DNAJB1^{WT} and DNAJB1^{H32Q} with or without crosslinking.
- Table S5 providing integrated TMT reporter ions and analysis for the effect of heat shock treatment on DNAJB1^{WT} and DNAJB1^{H32Q} AP-MS.

The mass spectrometry proteomics data and associated results files have been deposited to the ProteomeXchange Consortium via the PRIDE partner repository with the dataset identifier PXD030633.

AUTHOR INFORMATION

*To whom correspondence should be addressed: Joseph C. Genereux, 501 Big Springs Rd, Riverside, CA 92507. josephg@ucr.edu, 951-827-3759.

†Present Address: Department of Chemistry, Colgate University, Colgate, AZ

ACKNOWLEDGEMENTS

eGFP.pDEST30 plasmid was generously shared by R.L. Wiseman. This work was supported by a Society of Analytical Chemists of Pittsburgh Starter Grant (J.C.G.) and the University of California, Riverside.

CONFLICTS OF INTEREST

The authors declare that there is no conflict of interest.

ACCESSION CODES

DNAJB8: Uniprot entry Q8NHS0; DNAJB1: Uniprot entry P25685

REFERENCES

(1) Klaips, C. L., Jayaraj, G. G., and Hartl, F. U. (2018) Pathways of cellular proteostasis in aging and disease. *J. Cell Biol. 217*, 51–63.

(2) Sinnige, T., Yu, A., and Morimoto, R. I. (2020) Challenging Proteostasis: Role of the Chaperone Network to Control Aggregation-Prone Proteins in Human Disease, in *HSF1 and Molecular Chaperones in Biology and Cancer* (Mendillo, M. L., Pincus, D., and Scherz-Shouval, R., Eds.), pp 53–68. Springer International Publishing, Cham.

(3) Hipp, M. S., Kasturi, P., and Hartl, F. U. (2019) The proteostasis network and its decline in ageing. *Nat Rev Mol Cell Biol 20*, 421–435.

(4) Hu, J., Wu, Y., Li, J., Qian, X., Fu, Z., and Sha, B. (2008) The crystal structure of the putative peptide-binding fragment from the human Hsp40 protein Hdj1. *BMC Struct Biol 8*, 3.

(5) Söderberg, C. A. G., Månsson, C., Bernfur, K., Rutsdottir, G., Härmark, J., Rajan, S., Al-Karadaghi, S., Rasmussen, M., Höjrup, P., Hebert, H., and Emanuelsson, C. (2018) Structural modelling of the DNAJB6 oligomeric chaperone shows a peptide-binding cleft lined with conserved S/T-residues at the dimer interface. *Sci Rep 8*, 5199.

(6) Månsson, C., Kakkar, V., Monsellier, E., Sourigues, Y., Härmark, J., Kampinga, H. H., Melki, R., and Emanuelsson, C. (2014) DNAJB6 is a peptide-binding chaperone which can suppress amyloid fibrillation of polyglutamine peptides at substoichiometric molar ratios. *Cell Stress Chaperones 19*, 227–239.

(7) Hageman, J., Rujano, M. A., van Waarde, M. A. W. H., Kakkar, V., Dirks, R. P., Govorukhina, N., Oosterveld-Hut, H. M. J., Lubsen, N. H., and Kampinga, H. H. (2010) A DNAJB Chaperone Subfamily with HDAC-Dependent Activities Suppresses Toxic Protein Aggregation. *Molecular Cell 37*, 355–369.

(8) Karamanos, T. K., Tugarinov, V., and Clore, G. M. (2019) Unraveling the structure and dynamics of the human DNAJB6b chaperone by NMR reveals insights into Hsp40-mediated proteostasis. *Proc Natl Acad Sci USA 116*, 21529–21538.

(9) Karamanos, T. K., Tugarinov, V., and Clore, G. M. (2020) An S/T motif controls reversible oligomerization of the Hsp40 chaperone DNAJB6b through subtle reorganization of a β sheet backbone. *Proc Natl Acad Sci USA 117*, 30441–30450.

(10) Ryder, B. D., Matlahov, I., Bali, S., Vaquer-Alicea, J., van der Wel, P. C. A., and Joachimiak, L. A. (2021) Regulatory inter-domain interactions influence Hsp70 recruitment to the DnaJB8 chaperone. *Nat Commun 12*, 946.

(11) Rosenzweig, R., Nillegoda, N. B., Mayer, M. P., and Bukau, B. (2019) The Hsp70 chaperone network. *Nat Rev Mol Cell Biol*.

(12) Clerico, E. M., Tilitsky, J. M., Meng, W., and Gierasch, L. M. (2015) How Hsp70 Molecular Machines Interact with Their Substrates to Mediate Diverse Physiological Functions. *Journal of Molecular Biology 427*, 1575–1588.

(13) Craig, E. A., and Marszalek, J. (2017) How Do J-Proteins Get Hsp70 to Do So Many Different Things? *Trends Biochem. Sci. 42*, 355–368.

(14) Truman, A. W., Bourboulia, D., and Mollapour, M. (2021) Decrypting the chaperone code. *Journal of Biological Chemistry 296*, 100293.
(15) Kampinga, H. H., and Craig, E. A. (2010) The HSP70 chaperone machinery: J proteins as drivers of functional specificity (vol 11, pg 579, 2010). *Nature Reviews Molecular Cell Biology 11*.
(16) Kampinga, H. H., Andreasson, C., Barducci, A., Cheetham, M. E., Cyr, D., Emanuelsson, C., Genevaux, P., Gestwicki, J. E., Goloubinoff, P., Huerta-Cepas, J., Kirstein, J., Liberek, K., Mayer, M. P., Nagata, K., Nillegoda, N. B., Pulido, P., Ramos, C., De Los Rios, P., Rospert, S., Rosenzweig, R., Sahi, C., Taipale, M., Tomiczek, B., Ushioda, R., Young, J. C., Zimmermann, R., Zylicz, A., Zylicz, M., Craig, E. A., and Marszalek, J. (2019) Function, evolution, and structure of J-domain proteins. *Cell Stress Chaperones 24*, 7–15.
(17) Hageman, J., and Kampinga, H. H. (2009) Computational analysis of the human HSPH/HSPA/DNAJ family and cloning of a human HSPH/HSPA/DNAJ expression library. *Cell Stress Chaperones 14*, 1–21.
(18) Truman, A. W., Kristjansdottir, K., Wolfgeher, D., Ricco, N., Mayampurath, A., Volchenboum, S. L., Clotet, J., and Kron, S. J. (2015) Quantitative proteomics of the yeast Hsp70/Hsp90 interactomes during DNA damage reveal chaperone-dependent regulation of ribonucleotide reductase. *Journal of Proteomics 112*, 285–300.
(19) Taipale, M., Krykbaeva, I., Whitesell, L., Santagata, S., Zhang, J., Liu, Q., Gray, N. S., and Lindquist, S. (2013) Chaperones as thermodynamic sensors of drug-target interactions reveal kinase inhibitor specificities in living cells. *Nat Biotechnol 31*, 630–637.
(20) Quanrud, G. M., Montoya, M. R., Mei, L., Awad, M. R., and Genereux, J. C. (2021) Hsp40 Affinity to Identify Proteins Destabilized by Cellular Toxicant Exposure. *Anal Chem 93*, 16940–16946.
(21) Mei, L., Montoya, M. R., Quanrud, G. M., Tran, M., Villa-Sharma, A., Huang, M., and Genereux, J. C. (2020) Bait Correlation Improves Interactor Identification by Tandem Mass Tag-Affinity Purification-Mass Spectrometry. *J. Proteome Res. 19*, 1565–1573.
(22) Klock, H. E., and Lesley, S. A. (2009) The Polymerase Incomplete Primer Extension (PIPE) method applied to high-throughput cloning and site-directed mutagenesis. *Methods Mol Biol 498*, 91–103.
(23) Shoulders, M. D., Ryno, L. M., Genereux, J. C., Moresco, J. J., Tu, P. G., Wu, C., Yates, J. R., Su, A. I., Kelly, J. W., and Wiseman, R. L. (2013) Stress-Independent Activation of XBP1s and/or ATF6 Reveals Three Functionally Diverse ER Proteostasis Environments. *Cell Rep 3*, 1279–1292.
(24) Plate, L., Rius, B., Nguyen, B., Genereux, J. C., Kelly, J. W., and Wiseman, R. L. (2019) Quantitative Interactome Proteomics Reveals a Molecular Basis for ATF6-Dependent Regulation of a Destabilized Amyloidogenic Protein. *Cell Chem Biol 26*, 913-925.e4.
(25) Washburn, M. P., Wolters, D., and Yates, J. R. (2001) Large-scale analysis of the yeast proteome by multidimensional protein identification technology. *Nat Biotechnol 19*, 242–247.
(26) Zecha, J., Satpathy, S., Kanashova, T., Avanessian, S. C., Kane, M. H., Clauser, K. R., Mertins, P., Carr, S. A., and Kuster, B. (2019) TMT Labeling for the Masses: A Robust and Cost-efficient, In-solution Labeling Approach. *Mol Cell Proteomics 18*, 1468–1478.
(27) Chambers, M. C., Maclean, B., Burke, R., Amodei, D., Ruderman, D. L., Neumann, S., Gatto, L., Fischer, B., Pratt, B., Egertson, J., Hoff, K., Kessner, D., Tasman, N., Shulman, N., Frewen, B., Baker, T. A., Brusniak, M.-Y., Paulse, C., Creasy, D., Flashner, L., Kani, K., Moulding, C., Seymour, S. L., Nuwaysir, L. M., Lefebvre, B., Kuhlmann, F., Roark, J., Rainer, P., Detlev, S., Hemenway, T., Huhmer, A., Langridge, J., Connolly, B., Chadick, T., Holly, K., Eckels, J., Deutsch, E. W., Moritz, R. L., Katz, J. E., Agus, D. B., MacCoss, M., Tabb, D. L., and Mallick, P. (2012) A cross-platform toolkit for mass spectrometry and proteomics. *Nat Biotechnol 30*, 918–920.
(28) Kong, A. T., Leprevost, F. V., Avtonomov, D. M., Mellacheruvu, D., and Nesvizhskii, A. I. (2017) MSFragger: ultrafast and comprehensive peptide identification in mass spectrometry–based proteomics. *Nat Methods 14*, 513–520.

(29) da Veiga Leprevost, F., Haynes, S. E., Avtonomov, D. M., Chang, H.-Y., Shanmugam, A. K., Mellacheruvu, D., Kong, A. T., and Nesvizhskii, A. I. (2020) Philosopher: a versatile toolkit for shotgun proteomics data analysis. *Nat Methods 17*, 869–870.
(30) Mi, H., Ebert, D., Muruganujan, A., Mills, C., Albou, L.-P., Mushayamaha, T., and Thomas, P. D. (2021) PANTHER version 16: a revised family classification, tree-based classification tool, enhancer regions and extensive API. *Nucleic Acids Research 49*, D394–D403.
(31) Storey, J. D., and Tibshirani, R. (2003) Statistical significance for genomewide studies. *Proceedings of the National Academy of Sciences of the United States of America 100*, 9440–9445.
(32) Yekutieli, D., and Benjamini, Y. (1999) Resampling-based false discovery rate controlling multiple test procedures for correlated test statistics. *Journal of Statistical Planning and Inference 82*, 171–196.
(33) Mellacheruvu, D., Wright, Z., Couzens, A. L., Lambert, J. P., St-Denis, N. A., Li, T., Miteva, Y. V., Hauri, S., Sardiu, M. E., Low, T. Y., Halim, V. A., Bagshaw, R. D., Hubner, N. C., Al-Hakim, A., Bouchard, A., Faubert, D., Fermin, D., Dunham, W. H., Goudreault, M., Lin, Z. Y., Badillo, B. G., Pawson, T., Durocher, D., Coulombe, B., Aebersold, R., Superti-Furga, G., Colinge, J., Heck, A. J. R., Choi, H., Gstaiger, M., Mohammed, S., Cristea, I. M., Bennett, K. L., Washburn, M. P., Raught, B., Ewing, R. M., Gingras, A. C., and Nesvizhskii, A. I. (2013) The CRAPome: a contaminant repository for affinity purification-mass spectrometry data. *Nature Methods 10*, 730-+.
(34) Nishioka, K., and Reinberg, D. (2003) Methods and tips for the purification of human histone methyltransferases. *Methods 31*, 49–58.
(35) Piette, B. L., Alerasool, N., Lin, Z.-Y., Lacoste, J., Lam, M. H. Y., Qian, W. W., Tran, S., Larsen, B., Campos, E., Peng, J., Gingras, A.-C., and Taipale, M. (2021) Comprehensive interactome profiling of the human Hsp70 network highlights functional differentiation of J domains. *Molecular Cell 81*, 2549-2565.e8.
(36) Faust, O., Abayev-Avraham, M., Wentink, A. S., Maurer, M., Nillegoda, N. B., London, N., Bukau, B., and Rosenzweig, R. (2020) HSP40 proteins use class-specific regulation to drive HSP70 functional diversity. *Nature 587*, 489–494.
(37) Gillis, J., Schipper-Krom, S., Juenemann, K., Gruber, A., Coolen, S., van den Nieuwendijk, R., van Veen, H., Overkleeft, H., Goedhart, J., Kampinga, H. H., and Reits, E. A. (2013) The DNAJB6 and DNAJB8 Protein Chaperones Prevent Intracellular Aggregation of Polyglutamine Peptides. *J. Biol. Chem. 288*, 17225–17237.
(38) Rozales, K., Younis, A., Saida, N., Meller, A., Goldman, H., Kellerman, L., Heinrich, R., Berlin, S., and Shalgi, R. (2022) Differential roles for DNAJ isoforms in HTT-polyQ and FUS aggregation modulation revealed by chaperone screens. *Nat Commun 13*, 516.
(39) Huttlin, E. L., Bruckner, R. J., Navarrete-Perea, J., Cannon, J. R., Baltier, K., Gebreab, F., Gygi, M. P., Thornock, A., Zarraga, G., Tam, S., Szpyt, J., Gassaway, B. M., Panov, A., Parzen, H., Fu, S., Golbazi, A., Maenpaa, E., Stricker, K., Guha Thakurta, S., Zhang, T., Rad, R., Pan, J., Nusinow, D. P., Paulo, J. A., Schweppe, D. K., Vaites, L. P., Harper, J. W., and Gygi, S. P. (2021) Dual proteome-scale networks reveal cell-specific remodeling of the human interactome. *Cell 184*, 3022-3040.e28.
(40) Schweppe, D. K., Huttlin, E. L., Harper, J. W., and Gygi, S. P. (2018) BioPlex Display: An Interactive Suite for Large-Scale AP–MS Protein–Protein Interaction Data. *J. Proteome Res. 17*, 722–726.
(41) Otero, J. H., Lizák, B., Feige, M. J., and Hendershot, L. M. (2014) Dissection of Structural and Functional Requirements That Underlie the Interaction of ERdj3 Protein with Substrates in the Endoplasmic Reticulum. *J. Biol. Chem. 289*, 27504–27512.
(42) Moloney, T. C., Hoban, D. B., Barry, F. P., Howard, L., and Dowd, E. (2012) Kinetics of thermally induced heat shock protein 27 and 70 expression by bone marrow-derived mesenchymal stem cells: Heat Shock Protein Expression in MSC. *Protein Science 21*, 904–909.
(43) Diller, K. R. (2006) STRESS PROTEIN EXPRESSION KINETICS. *Annu. Rev. Biomed. Eng. 8*, 403–424.

(44) Jarzab, A., Kurzawa, N., Hopf, T., Moerch, M., Zecha, J., Leijten, N., Bian, Y., Musiol, E., Maschberger, M., Stoehr, G., Becher, I., Daly, C., Samaras, P., Mergner, J., Spanier, B., Angelov, A., Werner, T., Bantscheff, M., Wilhelm, M., Klingenspor, M., Lemeer, S., Liebl, W., Hahne, H., Savitski, M. M., and Kuster, B. (2020) Meltome atlas—thermal proteome stability across the tree of life. *Nat Methods 17*, 495–503.
(45) Leuenberger, P., Ganscha, S., Kahraman, A., Cappelletti, V., Boersema, P. J., von Mering, C., Claassen, M., and Picotti, P. (2017) Cell-wide analysis of protein thermal unfolding reveals determinants of thermostability. *Science 355*, eaai7825.
(46) Yu, H. Y., Ziegelhoffer, T., and Craig, E. A. (2015) Functionality of Class A and Class B J-protein co-chaperones with Hsp70. *FEBS Letters 589*, 2825–2830.
(47) Irwin, R., Faust, O., Petrovic, I., Wolf, S. G., Hofmann, H., and Rosenzweig, R. (2021) Hsp40s play complementary roles in the prevention of tau amyloid formation. *eLife 10*, e69601.
(48) McMahon, S., Bergink, S., Kampinga, H. H., and Ecroyd, H. (2021) DNAJB chaperones suppress destabilised protein aggregation via a region distinct from that used to inhibit amyloidogenesis. *Journal of Cell Science 134*, jcs255596.
(49) Savitski, M. M., Reinhard, F. B. M., Franken, H., Werner, T., Savitski, M. F., Eberhard, D., Molina, D. M., Jafari, R., Dovega, R. B., Klaeger, S., Kuster, B., Nordlund, P., Bantscheff, M., and Drewes, G. (2014) Tracking cancer drugs in living cells by thermal profiling of the proteome. *Science 346*, 1255784.